Diploma work on Master level

TRANSVERSE DYNAMICS
and
SYSTEM OVERVIEW FOR THE LEBT SECTION OF THE ESS LINAC

Author:
Sofia Louisy

Supervisor:
Natalia
Milas

Co-supervisors:
Mamad
Eshraqi

Joakim
Cederkäll

Lund University
Faculty of Science

2018-02-11

Abstract

The Low Energy Beam Transport, LEBT, is the first part of the European Spallation Source accelerator, the ESS linac, that is currently under construction in Lund. The LEBT section, that will be installed and commissioned in early 2018, has the purpose of focusing and steering the low-energy proton beam that enters directly from the ion source. For simulation of the beam dynamics in the LEBT, ESS uses the accelerator application library OpenXAL. This thesis presents the work in benchmarking models for the LEBT's focusing solenoids and steerers for OpenXAL, as well as the development of a user-friendly trajectory and envelope simulation application for the control room. Using TraceWin as a reference, the derived three-lenses approximation reduced the estimated worst case angle error of the steerers from 11.5% to 4.5% for the horizontal steerer and from 9.8% to 3.7% for the vertical steerer. Similar error reductions were found for the modified hard-edge model for the solenoids and the envelope evolution model. The LEBT application will be further developed by the Beam Physics section of ESS, and will finally be used in the control room during commissioning and routine operations of the LEBT.

Contents

Chapter 1

Introduction

The European Spallation Source, ESS, is currently under construction in the city of Lund, Sweden. Its 600-meter-long linear accelerator, linac, will enable new opportunities for research in materials and life sciences, energy and environmental technology, cultural heritage and fundamental physics. In the facility, high-energy neutrons will be produced using an accelerated proton beam at 96% of the speed of light that interacts with a tungsten target. The neutrons can thereafter interact on nuclear level with a sample, so that smaller and more complex material structures can be investigated. This makes the study of rare and biological samples, as well as samples under extreme conditions possible [1]. To do so, the facility has to be carefully planned and prepared. As part of this work, it is of high importance that the dynamics of the proton beam is understood so that the beam can be accurately transported.

The ESS linac consists of several different sections, all with specific tasks, through which the beam passes before reaching the tungsten target. The first part of the accelerator, right after the ion source, is a 2.5 meter section called Low Energy Beam Transport, or "LEBT". The aim of this section is to capture the diverging beam from the ion source. It must also transport a focused and aligned beam straight into the narrow opening of the next section of the accelerator, the Radio Frequency Quadrupole, or "RFQ". The protons in a low-energy beam are affected by the charge of their neighbours, and this space-charge effect causes a constant defocusing of the beam. To be able to serve its purpose of delivering a focused beam, the LEBT is equipped with two focusing solenoids. The extracted beam has also a risk of entering the LEBT off-axis due to possible misalignment of the ion source, or to be misaligned within the LEBT due to tilt of the LEBT elements. To be able to counteract misalignments, the LEBT is also equipped with steerers, which have the purpose of correcting a possible angle error.

As the LEBT is installed and commissioned, it is important to be able to analyse the beam trajectory and envelope evolution within the section. This is done by cross checking the beam properties using a trajectory and envelope simulation with the actual condition of the machine, which is read by two Non-invasive Profile Monitors (NPMs), one in between the two solenoids, and one at the end of the LEBT. The simulation tool can then be used to guide the operator on how to adjust the element parameters to reach a successful transport and focus of the beam into the RFQ. For a simulation tool to be developed at ESS, models of the beam dynamics in the LEBT need to be benchmarked and implemented into the accelerator application library OpenXAL.

The aim of this project is to benchmark solenoid, steerer and envelope models for OpenXAL, as well as to develop a user-friendly application that simulates the beam

centroid trajectory and the envelope throughout the LEBT. This application should have adjustable input parameters for the beam, as well as adjustable currents for the solenoids and steerers. It will serve as a first draft of the LEBT application.

This thesis gives an overview of the dynamics and specifications of the LEBT, together with a short description of the initial element models: the hard-edge model for the solenoids and the thin lens approximation for the steerers. It presents the methods and tools used for benchmarking and application development, and the corresponding final models together with error estimations. As there is no measurements to compare to at this stage, these errors were calculated with respect to simulations in the program TraceWin, that offers a possibility of using measured B-field values to create a more realistic element field map. It is shown that the new model, compared to the previous one, improves the beam position error from 17.0% to 3.4%, and the angle error from 64.0% to 12.7%, for a solenoid of 200 mT when compared to a field map simulation in TraceWin. Similarly, the steerer and envelope models are improved. The improved error from benchmarking of the new models led to the development of a beam simulation application of the LEBT, as this thesis' last part.

Chapter 2

The Low Energy Beam Transport

This chapter briefly introduces an overview of the LEBT, beam dynamics and describes the LEBT elements which this thesis concerns.

2.1 Overview

The ESS linac is 600 m long, and consists of a variety of sections, each with its own purpose (see Fig. 2.1). After the proton beam is extracted from the ion source, it will be accelerated to an energy of approximately 2 GeV (96% of the speed of light). The first section after the ion source is the 2.5 m long LEBT. In the LEBT, the beam energy is approximately 75 keV (1.3% of the speed of light), which qualifies the beam as non-relativistic. The purpose of the LEBT is to transport a focused beam straight into the next section, the RFQ, through a cone-shaped opening of 14 mm in diameter.

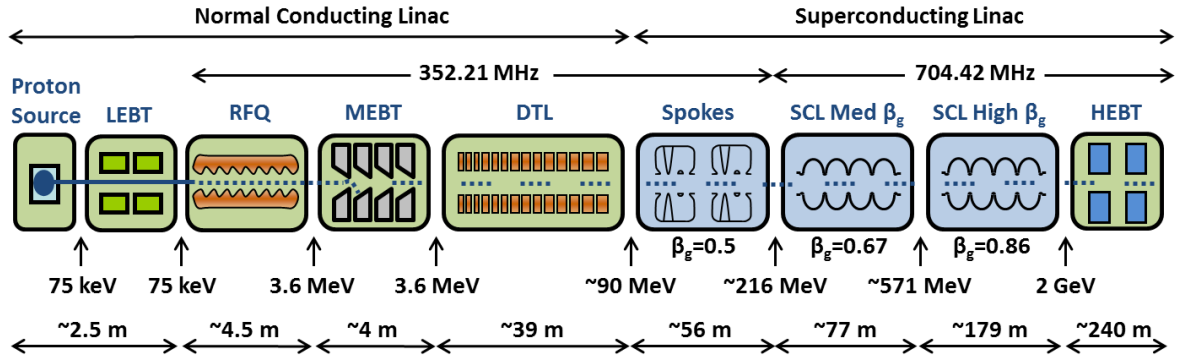

Figure 2.1: Schematic of the ESS linac [2].

The LEBT contains a variety of elements, such as solenoids, steerers, an iris, a chopper, a Faraday cup, an emittance-meter, a beam current transformer and a collimator, all of which are briefly described in Fig. 2.2. This thesis only considers the solenoids and the steerers, which focus and steers the proton beam.

2.2 Beam transport in the LEBT

Beam dynamics is the study of the collective behaviour of an ensemble of particles constituting the beam in a particle accelerator [4]. This section covers the equations of motion

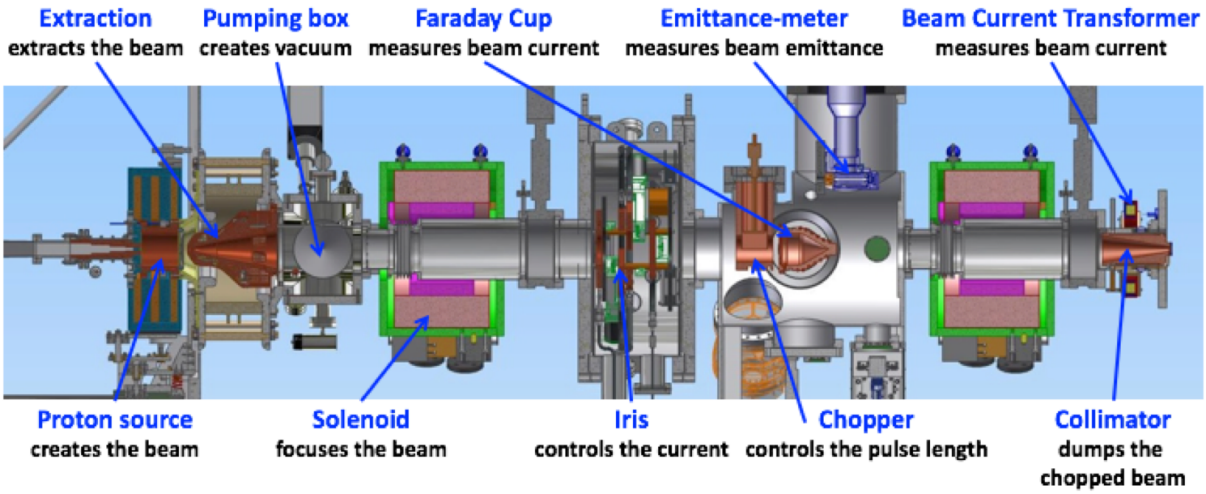

Figure 2.2: Ion source and the LEBT components. The steerers are positioned inside the solenoids [3].

for a particle in an external magnetic field, the transfer matrix formalism and the beam envelope that describes the space distribution of the beam. The collective state of a beam can be described by the beam emittance and Twiss parameters, which have to be given as an input parameter for the beam evolution in the LEBT.

A Cartesian coordinate system is used, where the z-axis defines the longitudinal direction, with origin at the start of the LEBT. The x-axis defines the horizontal transverse direction, and the y-axis defines the vertical transverse direction, both with origin relative to the z-axis, and moving with the particles.

The expected initial beam parameters have been simulated for the ion source and are presented in Table 2.1 [5].

Parameter	**Value**	**Unit**
Emittance ε_x	0.1223	π.mm.mrad
Twiss α_x	-3.303	-
Twiss β_x	0.397	mm/π.mrad
Emittance ε_y	0.1217	π.mm.mrad
Twiss α_y	-3.285	-
Twiss β_y	0.392	mm/π.mrad
Beam current	74	mA
Space charge compensation	0.95	-
Kinetic energy	75	keV
Relative speed, $\beta_r = v/c$	0.013	-
Lorentz factor, γ_r	1.000	-

Table 2.1: Expected beam parameters at the entrance of the LEBT [5].

2.2.1 Single-particle system

Equations of motion

The force from an external field on a particle is described by the Lorentz force [6],

$$\mathbf{F} = q(\mathbf{E} + \mathbf{v} \times \mathbf{B}), \tag{2.1}$$

where q is the charge, $\mathbf{v}$ is the velocity vector, $\mathbf{E}$ is the electric field and $\mathbf{B}$ is the magnetic field. This force, together with Newton's second law as $\mathbf{F} = d\mathbf{p}/dt$ [7], gives the equation of motion of the particle,

$$\frac{d\mathbf{p}}{dt} = q(\mathbf{E} + \mathbf{v} \times \mathbf{B}). \tag{2.2}$$

Within the LEBT, there are no forces acting in the longitudinal direction, which implies that the longitudinal equation of motion in the z-direction is simply that of a free particle. As there is no acceleration in the LEBT, $\mathbf{E} = 0$, and only the transverse equations of motion are therefore considered.

Let's first consider the magnitude of the horizontal acceleration; performing the curl in (2.2) gives,

$$\frac{dp_x}{dt} = q(v_y B_z - v_z B_y). \tag{2.3}$$

In the paraxial approximation, the transverse momentum components p_x and p_y are relatively small compared to p_z, so that $p_x, p_y \ll p_z$. The total momentum $p = \sqrt{p_x^2 + p_y^2 + p_z^2}$ can therefore be approximated as $p \approx p_z$ [8]. With $p \approx \gamma_r m v_z$, where γ_r is the relativistic Lorentz factor, m is the particle's rest mass and v_z is the particle velocity in the z-direction, the relative transverse momentums, or "angles", x' and y' are defined as,

$$\begin{aligned} x' &\equiv \frac{dx}{dz} \approx \frac{p_x}{p}, \\ y' &\equiv \frac{dyx}{dz} \approx \frac{p_y}{p}. \end{aligned} \tag{2.4}$$

Substituting the time derivative to a derivative in z as $d/dt = v_z d/dz$, where v_z is approximated to be a constant within the LEBT, (2.3) becomes,

$$x'' = \frac{q}{p}(B_z y' - B_y). \tag{2.5}$$

In the same manner, the vertical spacial acceleration is derived to be,

$$y'' = -\frac{q}{p}(B_z x' - B_x). \tag{2.6}$$

Typically, an accelerator does not contain elements that produce longitudinal magnetic fields, so $B_z = 0$. Also, the B_y-field in (2.5) can be expanded in a Taylor series around the origin,

$$B_y(z) = B_0(z)x + \frac{1}{2}\frac{\partial B(z)}{\partial x}x^2 + \dots. \tag{2.7}$$

Assuming x and y are small derivations with respect to the origin, and using only the first term in the expansion gives $B_y(z) \approx B_0(z)x$, and $B_x(z) \approx B_0(z)y$. The equations of motion then becomes,

$$\begin{aligned} x'' + k_x^2 x &= 0, \\ y'' + k_y^2 y &= 0, \end{aligned} \tag{2.8}$$

with $k_a^2 \equiv qB_0(z)/p$, where $a \in \{x, y\}$.

These equations resemble the dynamics of a simple harmonic oscillator [9]. Making this *Ansatz*, remembering that $k_a = k_a(z)$, the equations can be given a similar solution,

$$\begin{cases} x(z) &= x_0 \cos(k_x z) + \frac{x_0'}{k_x} \sin(k_x z) \\ x'(z) &= -k_x x_0 \sin(k_x z) + x_0' \cos(k_x z) \\ y(z) &= y_0 \cos(k_y z) + \frac{y_0'}{k_y} \sin(k_y z) \\ y'(z) &= -k_y y_0 \sin(k_y z) + y_0' \cos(k_y z) \end{cases}. \tag{2.9}$$

Transfer matrix formalism

The transverse state of a particle can be described as a phase space vector,

$$P = \begin{pmatrix} x \\ x' \\ y \\ y' \end{pmatrix}. \tag{2.10}$$

With this vector, the linear matrix that transfers the state from one point to another, $P(z) = MP(0)$, is constructed from (2.9) to be,

$$M = \begin{pmatrix} \cos(k_x z) & \frac{1}{k_x}\sin(k_x z) & 0 & 0 \\ -k_x \sin(k_x z) & \cos(k_x z) & 0 & 0 \\ 0 & 0 & \cos(k_y z) & \frac{1}{k_y}\sin(k_y z) \\ 0 & 0 & -k_x \sin(k_y z) & \cos(k_y z) \end{pmatrix}. \tag{2.11}$$

This matrix can now be used as a basis to construct the transfer matrix for different elements.

Example I: Drift In a drift space, no external fields are present, so $k_x = k_y = 0$. The elements of (2.11) then becomes,

$$\begin{aligned} \cos(k_a z) &\to 1, \\ \sin(k_a z) &\to 0, \\ \frac{\sin(k_a z)}{k_a} &\to z. \end{aligned}$$

For a drift length of L, the resulting matrix is therefore,

$$M_{\text{drift}} = \begin{pmatrix} 1 & L & 0 & 0 \\ 0 & 1 & 0 & 0 \\ 0 & 0 & 1 & L \\ 0 & 0 & 0 & 1 \end{pmatrix}. \tag{2.12}$$

This results in the following transfer,

$$\begin{pmatrix} x \\ x' \\ y \\ y' \end{pmatrix} = M_{\text{drift}} \begin{pmatrix} x_0 \\ x_0' \\ y_0 \\ y_0' \end{pmatrix} = \begin{pmatrix} x_0 + x_0' L \\ x_0' \\ y_0 + y_0' L \\ y_0' \end{pmatrix}. \tag{2.13}$$

Example II: Quadrupole For a focusing quadrupole in the thin lens approximation, $k_x^2 L = f^{-1}$ while $k_y^2 L = -f^{-1}$, where L is the length of the quadrupole, approximated to be infinitely thin, and f is the focal length [10]. As $L \to 0$, the elements of (2.11) become,

$$\begin{aligned} \cos(k_a z) &\to 1, \\ \sin(k_a z) &\to 0, \\ k_a \sin(k_a z) &= k_a^2 L - \frac{k^4 L^3}{3!} + \cdots \to 1/f, \end{aligned}$$

which gives the matrix

$$M_{\text{quad}} = \begin{pmatrix} 1 & 0 & 0 & 0 \\ -\frac{1}{f} & 1 & 0 & 0 \\ 0 & 0 & 1 & 0 \\ 0 & 0 & \frac{1}{f} & 1 \end{pmatrix}. \tag{2.14}$$

This results in a transfer,

$$\begin{pmatrix} x \\ x' \\ y \\ y' \end{pmatrix} = M_{\text{quad}} \begin{pmatrix} x_0 \\ x_0' \\ y_0 \\ y_0' \end{pmatrix} = \begin{pmatrix} x_0 \\ x_0' - f^{-1} x_0 \\ y_0 \\ y_0' + f^{-1} y_0 \end{pmatrix}. \tag{2.15}$$

Note that if the beam is focused in one direction, it is automatically defocused in the other. To achieve net focusing with quadrupoles, at least 2 elements are therefore needed.

Both the drift and the quadrupole matrices are filled with zero in their off-diagonal elements. Non-zero elements would indicate a coupling between the horizontal and vertical components [11], which will be seen in the transfer matrix of the solenoid in section 2.3.1.

2.2.2 Multi-particle system

Envelope

The envelope represents the edge of the space distribution of a beam, while the centroid represents the statistical mean position of the particles. The envelope is typically a multiple of the root mean square, RMS, of the distribution. Instead of performing full multi-particle simulations when predicting the beam, these statistical properties can instead be used, which results in a less time-consuming program.

The Transversal RMS's are calculated as,

$$\sigma_x = \sqrt{\langle x^2 \rangle - \langle x \rangle^2}, \qquad \sigma_y = \sqrt{\langle y^2 \rangle - \langle y \rangle^2}, \tag{2.16}$$

where $\langle x^2 \rangle$ and $\langle y^2 \rangle$ are the mean values of all the particle positions squared, and $\langle x \rangle^2$ and $\langle y \rangle^2$ are the square of the mean value of all the particle positions.

Depending on the distribution shape, the RMS includes a different fraction of the beam. For a Gaussian distribution, the RMS envelope (2σ) contains 68.3% of the beam. To include a larger portion of this beam, the envelope is scaled by the RMS size, where scaling the envelope to four times the RMS instead includes 95% of the beam [12].

Beam emittance, covariance matrix and Twiss parameters

The collective state of a beam can be described by the beam emittance and Twiss density parameters, which together give the particle distribution in phase space. In phase space, the particle density is plotted as a point, with the angle against the position. The expected phase-space distribution for the input beam of the LEBT can be seen in Fig. 2.3.

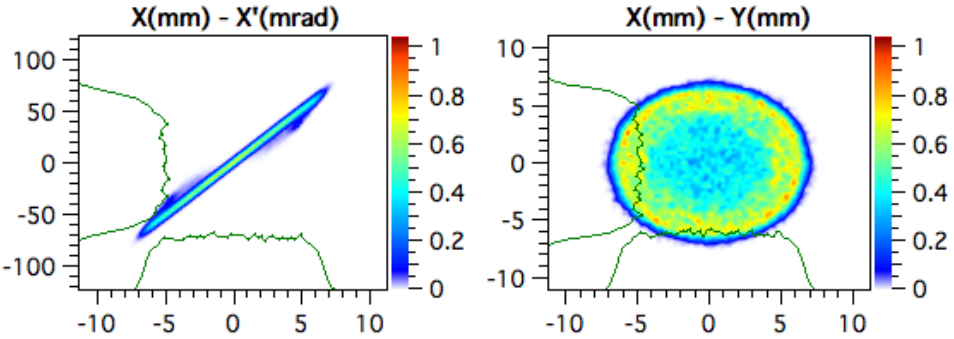

Figure 2.3: (left) Expected LEBT input distribution in phase space and (right) its corresponding space distribution. The color bar represents the particle density. The beam is expected to be transversely symmetric, so that $x - x' = y - y'$.

The distribution in phase space generally forms an ellipse. The shape of this ellipse is described by the statistical phase-space RMS distribution as a covariance matrix,

$$\Sigma_x = \langle \mathbf{X}\mathbf{X}^T \rangle = \begin{pmatrix} \langle x^2 \rangle & \langle xx' \rangle \\ \langle x'x \rangle & \langle x'^2 \rangle \end{pmatrix}. \tag{2.17}$$

Here,

$$\mathbf{X} = \begin{pmatrix} x \\ x' \end{pmatrix}$$

is the phase space vector of each particle in one dimension. The area of the ellipse is calculated from the determinant of the covariance matrix as,

$$\text{Area} = \pi[\det(\Sigma_x)]^{1/2} = \pi\varepsilon_x, \tag{2.18}$$

where ε_x is the horizontal emittance, defined as,

$$\varepsilon_x \equiv [\langle x^2 \rangle \langle x'^2 \rangle - \langle xx' \rangle^2]^{1/2} \tag{2.19}$$

$$= [\det(\Sigma_x)]^{1/2}. \tag{2.20}$$

The evolution of the covariance matrix is described as,

$$\Sigma_{x,1} = M\Sigma_{x,0}M^T, \tag{2.21}$$

where M is the transfer matrix described in (2.11). This gives the evolution of the emittance as,

$$\begin{aligned} \varepsilon_{x,z} &= [\det(M\Sigma_{x,0}M^T)]^{1/2} \\ &= [\det(M)\det(\Sigma_{x,0})\det(M^T)]^{1/2}. \end{aligned} \tag{2.22}$$

When there is no acceleration of the beam, and all the forces acting on the beam are linear, the transfer matrices are unitary, so that $\det(M) = \det(M^T) = 1$ [13]. $\varepsilon_{x,z}$ then becomes,

$$\begin{aligned} \varepsilon_{x,z} &= [\det(\Sigma_{x,0})]^{1/2} \\ &= \varepsilon_{x,0}. \end{aligned} \tag{2.23}$$

The emittance is hence an invariant of motion. This follows Liouville's theorem, that states that the emittance, that is proportional to the Hamiltonian (the energy) of the system, stays constant along the trajectories of a Hamiltonian system [13, 14]. A loss in beam quality results in an increase of the emittance.

Since the emittance and hence the area is ideally constant, it is natural to redefine the covariance matrix as,

$$\Sigma = \varepsilon \mathbf{T}, \tag{2.24}$$

where

$$\mathbf{T} \equiv \begin{pmatrix} \beta & -\alpha \\ -\alpha & \gamma \end{pmatrix}, \tag{2.25}$$

and $(\det \mathbf{T} = 1)$. The elements of the normalized matrix $\mathbf{T}$ are the Courant-Snyder parameters, or the Twiss parameters [15], defined as,

$$\begin{aligned} \sqrt{\beta_x \varepsilon_x} &\equiv \langle x^2 \rangle^{1/2}, \\ \alpha_x \varepsilon_x &\equiv -\langle x x' \rangle, \\ \sqrt{\gamma_x \varepsilon_x} &\equiv \langle x'^2 \rangle^{1/2}, \end{aligned} \tag{2.26}$$

where $\gamma_x = (1 + \alpha_x^2)/\beta_x$. Note that β_x and γ_x differ from the relative speed β_r and the Lorentz factor γ_r. The Twiss parameters are a convention, which describes the shape and evolution of the ellipse. α_x, β_x and γ_x can all be transported along the beamline with the same transfer matrices as the beam centroid (see Fig. 2.4). All derived equations apply in the same way for the $y - y'$ plane.

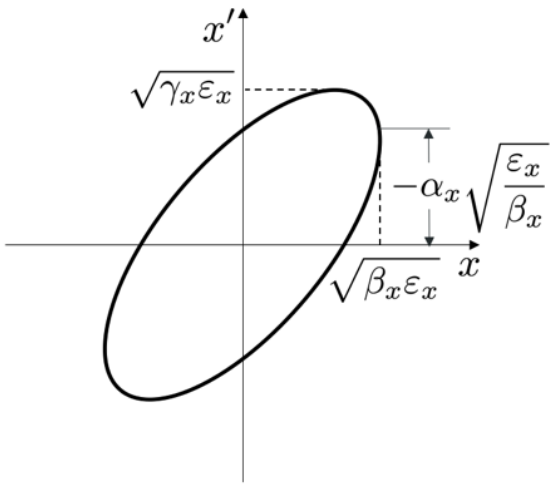

Figure 2.4: The phase space ellipse with the shape-defining Twiss parameters [16].

Space charge

When a beam consists of charged particles, they will naturally repel each other. This causes a defocusing of the beam. However, this space charge effect has different significance for low-energy and high-energy beams.

Consider a uniform cylindrical beam. If there are N particles per unit length in a beam radius a, then the produced electrical and magnetic fields inside the beam ($r < a$) are,

$$E_r = \frac{qN}{2\pi\epsilon_0 a^2} r, \tag{2.27}$$

$$B_\phi = \frac{qNv}{2\pi\epsilon_0 a^2 c^2} r, \tag{2.28}$$

where ϵ_0 is the permittivity in vacuum and c is the speed of light. The net force on a particle is then derived from the Lorentz force as,

$$F_(r) = \frac{q^2 N}{2\pi\epsilon_0 a^2 \gamma_r^2} r, \tag{2.29}$$

where $\gamma_r = (1 - \beta_r^2)^{-1}$ is the Lorentz factor and $\beta_r = v/c$ is the relative speed. If the beam instead has symmetrical Gaussian distribution, the force becomes,

$$F_G(r) = \frac{q^2 N}{2\pi\epsilon_0 \gamma_r^2 r}(1 - e^{-r^2/2\sigma^2}). \tag{2.30}$$

where σ is the RMS of the Gaussian distribution.

For high-energy beams, γ_r is large, and the space charge force becomes negligible. As the LEBT transports a low-energy beam, this force is not negligible and causes the beam to constantly defocus. The space charge force therefore results in a loss in beam quality within the LEBT. To reduce this defocusing, the LEBT is designed with a lower vacuum (higher pressure). The beam has a chance of ionizing a gas, after which the negative ions will be attracted to the beam while the positive ions are repelled. The negative ions will then compensate for a part of the charge. This is called space charge compensation.

2.3 LEBT elements

2.3.1 Solenoid

The focusing elements in the LEBT consists of two solenoids. A solenoid can provide transverse focusing in both the horizontal and vertical direction simultaneously. This means that a solenoid takes less space as a focusing element compared to quadrupoles, that require a combination of at least two elements for both horizontal and vertical focusing. However, a solenoid also couples the horizontal and vertical component of the beam, which makes the dynamics slightly more complicated than for a quadrupole.

A solenoid is an electromagnetic element that consists of a coil wound into a tightly packed helix, see Fig. 2.5. The produced magnetic field consists of a longitudinal component, B_z, that dominates the body of the solenoid. To obey Maxwell's equations and conserve the magnetic flux, the field diverges radially at the edges of the solenoid as the longitudinal field drops [17].

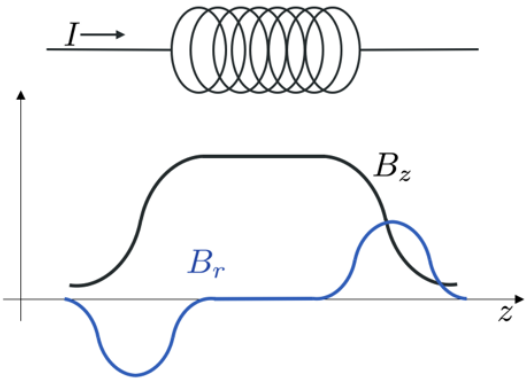

Figure 2.5: (Top) Wire outline of a solenoid, where the arrow indicates a longitudinal (z-) direction. (Bottom) Typical longitudinal magnetic field (B_z) and radial magnetic field (B_r).

Since a realistic field model is complicated to describe mathematically, a simplified "hard-edge" model is used. In the hard-edge model, the body of the solenoid produces a constant longitudinal field, $B_z = B_0$. The fringe field at the edges is considered to be defined within an infinitely short region, Δl, between two planes. To obey Gauss law of magnetic flux, $B_r = B_z' r/2$ in this region, which gives the acceleration in the horizontal direction from (2.5) as,

$$x'' = \frac{q}{p}(y' B_z + \frac{y}{2} B_z') \tag{2.31}$$

$$= \frac{q}{2p}\left((y B_z)' + y' B_z\right). \tag{2.32}$$

Integrating this for the entrance of the solenoid from $z = 0$ to $z = \Delta l$ gives the angular kick $\Delta x' = x'(\Delta l) - x'(0)$ as,

$$\Delta x' = \frac{q}{2p}\left((y B_z)|_0^{\Delta l} + \int_0^{\Delta l} y' B_z dz\right) \tag{2.33}$$

$$= \frac{q}{2p}\left(y B_0 + \int_0^{\Delta l} y' B_z dz\right). \tag{2.34}$$

Assuming a linear longitudinal field in this region, $B_z = B_0 z/\Delta l$, the latter term in (2.34) vanishes as Δl goes to zero,

$$\lim_{\Delta l \to 0} \frac{B_0}{\Delta l} \int_0^{\Delta l} y' z \, dz = \lim_{\Delta l \to 0} B_0 y'(\Delta l) \Delta l = 0. \tag{2.35}$$

Calculating the vertical kick in the same manner gives the angular transformation of the entrance of the solenoid,

$$x' \to x' + k_s y, \tag{2.36}$$

$$y' \to y' - k_s x. \tag{2.37}$$

where $k_s \equiv qB_0/2p$.

This result indicates that any vertical offset of an incoming particle results in an added horizontal angle, and vice versa. Hence, a coupling between a particle's horizontal and

vertical components is created already at the solenoid's entrance. In this lens approximation, the particle trajectory must be continuous, so with eq. (2.36-2.37), the transfer matrix of the solenoid's entrance is constructed to be,

$$M_{\text{enter}} = \begin{pmatrix} 1 & 0 & 0 & 0 \\ 0 & 1 & k_s & 0 \\ 0 & 0 & 1 & 0 \\ -k_s & 0 & 0 & 1 \end{pmatrix}. \tag{2.38}$$

At the exit of the solenoid, the radial field points in the opposite direction (see Fig. 2.5), so that $k_s \to -k_s$, which gives the exit transfer matrix,

$$M_{\text{exit}} = \begin{pmatrix} 1 & 0 & 0 & 0 \\ 0 & 1 & -k_s & 0 \\ 0 & 0 & 1 & 0 \\ k_s & 0 & 0 & 1 \end{pmatrix}. \tag{2.39}$$

In the body of the solenoid, $B_x = B_y = 0$, while $B_z = B_0$. From (2.5), the acceleration is be expressed as,

$$\frac{d}{dz}\begin{pmatrix} x' \\ y' \end{pmatrix} = 2k_s \begin{pmatrix} 0 & 1 \\ -1 & 0 \end{pmatrix}\begin{pmatrix} x' \\ y' \end{pmatrix}. \tag{2.40}$$

Integrating this from $z = 0$ to $z = L$ gives the angle transformation,

$$\begin{pmatrix} x'(L) \\ y'(L) \end{pmatrix} = \begin{pmatrix} \cos(2k_sL) & \sin(2k_sL) \\ -\sin(2k_sL) & \cos(2k_sL) \end{pmatrix}\begin{pmatrix} x'(0) \\ y'(0) \end{pmatrix}. \tag{2.41}$$

As can be seen in (2.41), any transverse angular component of a passing particle will cause the particle to continuously rotate around the longitudinal field lines, with a radius that is proportional to the transverse angular component $r' = \sqrt{x'^2 + y'^2}$. A second integration gives the trajectory transformation,

$$\begin{pmatrix} x(L) \\ y(L) \end{pmatrix} = \begin{pmatrix} x(0) \\ y(0) \end{pmatrix} + \frac{1}{2k_s}\begin{pmatrix} \sin(2k_sL) & 2\sin^2(k_sL) \\ -2\sin^2(k_sL) & \sin(2k_sL) \end{pmatrix}\begin{pmatrix} x'(0) \\ y'(0) \end{pmatrix}, \tag{2.42}$$

which is combined with (2.41) to form the transfer matrix for the solenoid body as,

$$M_{\text{body}} = \begin{pmatrix} 1 & \frac{1}{2k_s}\sin(2k_sL) & 0 & \frac{1}{k_s}\sin^2(k_sL) \\ 0 & \cos(2k_sL) & 0 & \sin(2k_sL) \\ 0 & -\frac{1}{k_s}\sin^2(k_sL) & 1 & \frac{1}{2k_s}\sin(2k_sL) \\ 0 & -\sin(2k_sL) & 0 & \cos(2k_sL) \end{pmatrix}. \tag{2.43}$$

The three solenoid parts: entrance, body and exit, are now combined to form a complete transfer matrix, M_{sol}, for the solenoid as,

$$M_{\text{sol}} = M_{\text{exit}}M_{\text{body}}M_{\text{enter}} = \begin{pmatrix} \cos^2(k_sL) & \frac{1}{2k_s}\sin(2k_sL) & \frac{1}{2}\sin(2k_sL) & \frac{1}{k_s}\sin^2(k_sL) \\ -\frac{k_s}{2}\sin(2k_sL) & \cos^2(k_sL) & -k_s\sin^2(k_sL) & \frac{1}{2}\sin(2k_sL) \\ -\frac{1}{2}\sin(2k_sL) & -\frac{1}{k_s}\sin^2(k_sL) & \cos^2(k_sL) & \frac{1}{2k_s}\sin(2k_sL) \\ k_s\sin^2(k_sL) & -\frac{1}{2}\sin(2k_sL) & -\frac{k_s}{2}\sin(2k_sL) & \cos^2(k_sL) \end{pmatrix}. \tag{2.44}$$

The non-zero off-diagonal elements of the solenoid's transfer matrix indicate a coupling between the horizontal and vertical components of the beam.

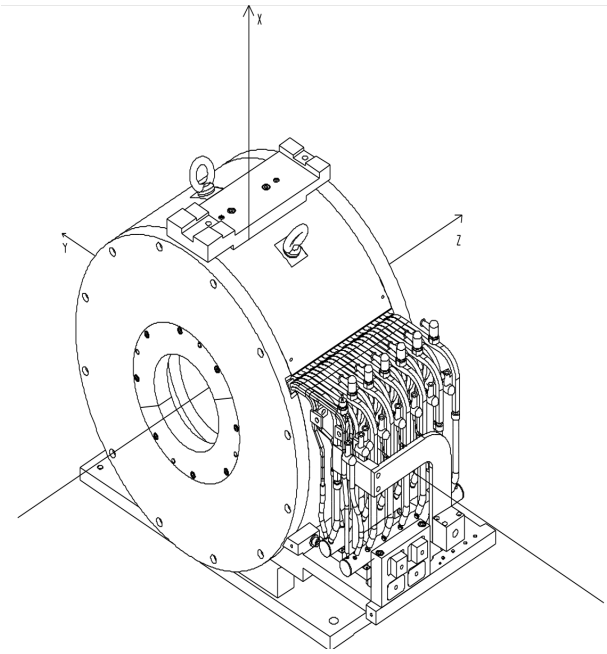

Figure 2.6: Schematics of the LEBT solenoid [19].

Another interesting way of composing this matrix is as a combination of a rotation and a focusing element [18],

$$M_{\text{sol}} = RM_f = M_f R, \tag{2.45}$$

where

$$R = \begin{pmatrix} \mathbf{I}\cos(k_s L) & \mathbf{I}\sin(k_s L) \\ -\mathbf{I}\sin(k_s L) & \mathbf{I}\cos(k_s L) \end{pmatrix}, \qquad \mathbf{I} = \begin{pmatrix} 1 & 0 \\ 0 & 1 \end{pmatrix} \tag{2.46}$$

$$M_f = \begin{pmatrix} F & \mathbf{0} \\ \mathbf{0} & F \end{pmatrix}, \qquad \mathbf{0} = \begin{pmatrix} 0 & 0 \\ 0 & 0 \end{pmatrix} \tag{2.47}$$

$$F = \begin{pmatrix} \cos(k_s L) & \frac{1}{k_s}\sin(k_s L) \\ -k_s \sin(k_s L) & \cos(k_s L) \end{pmatrix}. \tag{2.48}$$

The solenoid gives a total rotation of $\phi = k_s L$, while the focal length of the solenoid is derived by compressing (2.48) in the thin lens approximation. As $L \to 0$, the inverse focal length is given by the first term of the limit

$$\lim_{L\to 0} k_s \sin(k_s L) \approx k_s^2 L = 1/f. \tag{2.49}$$

So, for a solenoid, $f \propto p^2$, while as we have seen for a quadrupole $f = (k_x^2 L)^{-1} \propto p$. Hence, the solenoid is more efficient as a focusing element for a low-energy beam than a quadrupole, since the focal length of a solenoid can be assumed to be shorter.

Specifications for the LEBT solenoid

A drawing of the LEBT solenoid can be seen in Fig. 2.6 and specifications can be seen in Table.2.2.

Parameter	Value	Unit
Length	0.240	m
Radius	125	mm
Maximum B_{peak}	408	mT

Table 2.2: Solenoid specifications.

2.3.2 Steerer

The LEBT is equipped with horizontal and vertical steerers, that are placed inside the solenoids.

A steerer is an element that produces a transverse magnetic field, where a horizontal steerer produces a field in the y-direction, while a vertical produces a field in the x-direction. In contrast to a dipole, the intention of a steerer is to give the charged particle an angular kick without changing the reference trajectory. A convenient approximation for the steerer is to describe it as a thin lens.

The total kick from a steerer is calculated from its integrated magnetic field,

$$BL = \int_{-\infty}^{\infty} B_{\text{field}}(z)dz, \tag{2.50}$$

where the kick will be in a direction perpendicular to both the field and the particle's trajectory, and is approximated to be independent of the particle's transversal state. The kick is concentrated at the centre of the element, where the horizontal and vertical steerer gives an angular kick of,

$$dx' = -\frac{q}{p}(BL)_h \qquad \text{and} \qquad dy' = \frac{q}{p}(BL)_v. \tag{2.51}$$

The angular transformation through the steerers will then be $x' \to x' + dx'$ for the horizontal steerer, and $y' \to y' + dy'$ for the vertical steerer. In the thin lens approximation, the trajectory must stay continuous

One way to express this effect is to expand the phase space vector P, so that,

$$P \to \begin{pmatrix} x \\ x' \\ y \\ y' \\ 1 \end{pmatrix}. \tag{2.52}$$

This allows a transfer matrix to be constructed as,

$$M_{\text{kick}} = \begin{pmatrix} 1 & 0 & 0 & 0 & 0 \\ 0 & 1 & 0 & 0 & dx' \\ 0 & 0 & 1 & 0 & 0 \\ 0 & 0 & 0 & 1 & dy' \\ 0 & 0 & 0 & 0 & 1 \end{pmatrix}. \tag{2.53}$$

The transfer then becomes,

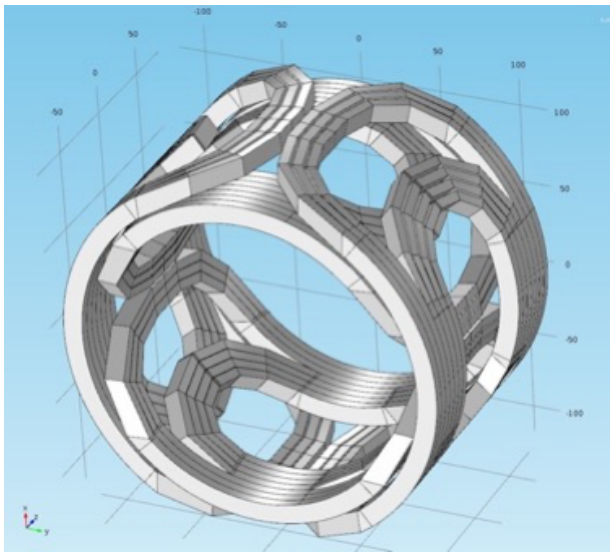

Figure 2.7: Model of the LEBT steerers, where the vertical steerer is the inner construction, and the horizontal is the outer. The steerers are positioned inside the solenoid [3].

$$\begin{pmatrix} x \\ x' \\ y \\ y' \\ 1 \end{pmatrix} = M_{\text{kick}} \begin{pmatrix} x_0 \\ x'_0 \\ y_0 \\ y'_0 \\ 1 \end{pmatrix} = \begin{pmatrix} x_0 \\ x'_0 + dx' \\ y_0 \\ y'_0 + dy' \\ 1 \end{pmatrix} \tag{2.54}$$

In a simulation where a steerer is used, the transfer matrices of other elements can easily be adjusted to this new phase space vector through an identity expansion.

Specifications for the LEBT steerers

A model of the steerers can be seen in Fig. 2.7 and specifications of the steerers can be seen in Table 2.3.

Parameter	**Value**	**Unit**
Length	0.320	m
Maximum B_{peak}, H-steerer	8.6	mT
Maximum B_{peak}, V-steerer	10.3	mT
Maximum horizontal kick	-35.3	mrad
Maximum vertical kick	40.4	mrad

Table 2.3: Steerer specifications. The horizontal steerer has a lower kick maximum amplitude due to the fact that it is positioned outside of the vertical steerer.

Chapter 3

Methods

In order for the LEBT to serve its purpose and transport the proton beam from the source with a sharp focus straight into the entrance of the RFQ, it is important to be able to find the optimal element parameters. During commissioning, these parameters will be found using live-readings from the NPMs (Non-invasive Profile Monitors), Faraday cups and emittance monitor units placed inside and outside the LEBT, together with a user-friendly beam trajectory and envelope simulation application. For this application to be written, models need to be benchmarked for the elements in the LEBT. This thesis benchmarks models for the solenoids, steerers and the envelope of the beam, as well as provides a first draft of the LEBT application.

To get a better understanding of the trajectory simulation, it was written in the program language Python, using the hard-edge model for the solenoids and the thin lens approximation for the steerers. The hard-edge model for the solenoid, and the thin lens approximation was then simulated in the development environment OpenXAL, from where the errors were quantified, and the models were then improved using different strategies. The simulation program TraceWin was used as a reference for the error calculations. A user-friendly simulation program was then written in the software platform JavaFX. The mentioned software tools are described in more detail below.

3.1 Software tools

TraceWin

TraceWin is a simulation program that calculates the beam dynamics in particle accelerators, where the different elements of the linac can be modelled either by using analytic expression or field maps created from the element's field profile [20]. TraceWin also has the ability to overlap field maps, making the simulation of several overlapped elements as realistic as possible. There are no experimental data in this thesis, and therefore, field map simulations in TraceWin were used as a reference for benchmarking element models as the envelope and trajectory calculations were done in OpenXAL.

OpenXAL

OpenXAL is a Java-based open source developement environment used for creating accelerator physics applications, scripts and services [21]. ESS uses this library do develop applications for the control room, and is hence where the simulation of the beam dynamics

occurred. This is the program for which the models need to be benchmarked. OpenXAL was not developed to handle element field maps, but during the work of this thesis, a version was released where the solenoid field map could be used.

Python

Python is a high-level programming language for general-purpose programming [22]. As Python is a language in which it is easy to perform calculations and plotting, JPype was used to link OpenXAL to Python to make it easier to work with. It was also used to calculate a more accurate transfer matrix for the solenoid, and to quantify errors.

JavaFX API

JavaFX is a software platform, based on the programming language Java, for creation of desktop applications [23]. As OpenXAL is based on Java, it was then a natural choice to make the application program interface using Java. Gluon's Scene builder was used with JavaFX for creation of the interface [24], while the actions were written in Java code.

Chapter 4

Results

4.1 Trajectory simulation

To get a better understanding of the dynamics, a simulation for the LEBT was written with Python code using hard-edge models for the solenoids, and steerers as thin lenses in the middle of the solenoids. The code is presented in Appendix I. This code was compared with TraceWin for benchmarking and comparison.

4.2 Solenoid in the hard-edge model

The hard-edge model is an efficient way of describing a solenoid. It is easy to calculate and has in most cases an acceptable accuracy [25]. The model simplifies the magnetic field map of an element to the shape of a box, with the height, B_0, being the maximum B-field and a length L, which together multiplies to the same total magnetic integral as the real field on axis,

$$B_0 L = \int_{-\infty}^{\infty} B_{\text{field}}(z) dz. \tag{4.1}$$

The hard-edge model is convenient for a solenoid which has a recognizable flat top gradient [25]. The LEBT solenoids are short in comparison with their radius, which results in a field without a well defined plateau. The consequence of this is that this original (old) hard-edge model results in an inaccurate beam centroid trajectory when compared to a TraceWin field map simulation. This thesis' work around the solenoids was aimed to increase the accuracy of the hard-edge model for the LEBT solenoids.

Helmut Weidemann presents a procedure for defining a more accurate transfer matrix for a quadrupole through a step function [11]. In the same manner, the solenoid field map with a typical peak field of 235 mT was decomposed into segments (see Fig. 4.1), where each segment was described separately by a hard-edge model. The transfer matrices of each hard-edge model, M_i, were then multiplied together to form one single transfer matrix,

$$M_{\text{sol}} = M_N M_{N-1} \dots M_1. \tag{4.2}$$

The Python code for this segmentation can be seen in Appendix II. The matrix elements were then compared with the hard-edge transfer matrix described in (2.44) to retrieve a new and improved set of parameters B_0 and L. This matrix procedure was then repeated for a solenoid of a peak field strength ranging between 100 and 400 mT, and the resulting parameters can be seen in the plot in Fig. 4.2. From the calculated parameters, a new

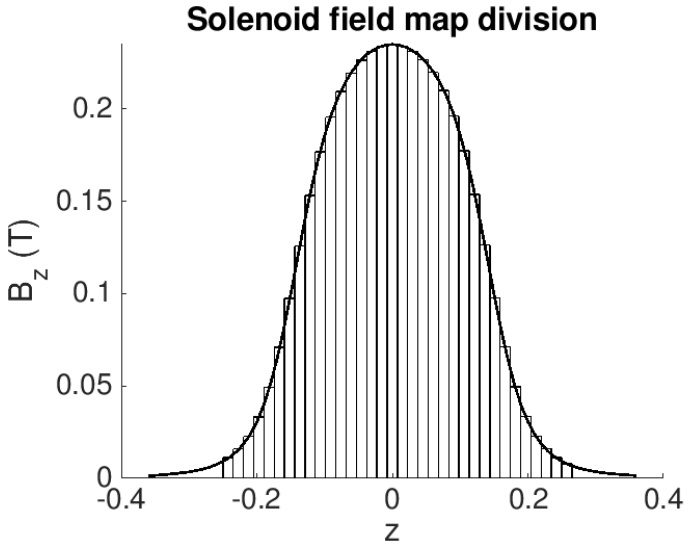

Figure 4.1: Segmentation of the solenoid field map into hard-edge models.

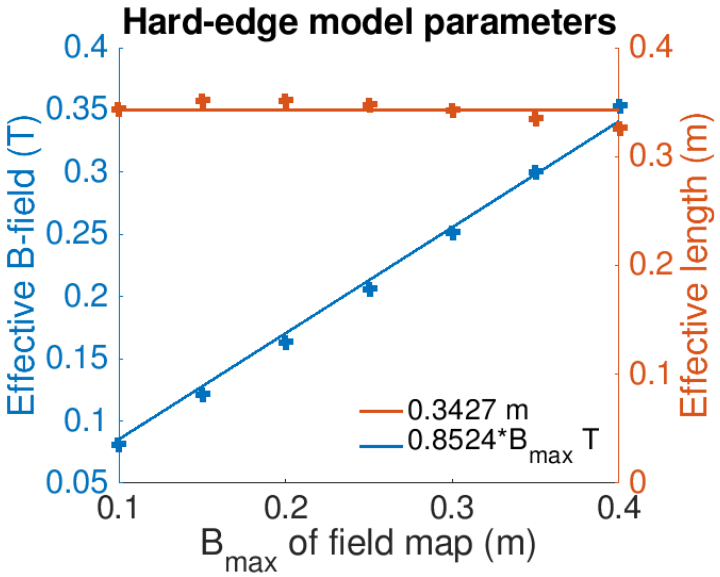

Figure 4.2: Ideal hard-edge parameters for different field strengths of the LEBT solenoids, together with a constant and linear fit.

length was determined as the average of all results, while the new field was determined as a linear fit, giving the new parameters,

$$L_{\text{new}} = 342.7 \text{ mm}, \tag{4.3}$$
$$B_{\text{new}} = 0.8524 \cdot B_0 \text{ T}. \tag{4.4}$$

This can be compared with the parameters of the old hard-edge model,

$$L_{\text{old}} = 284.1 \text{ mm}, \tag{4.5}$$
$$B_{\text{old}} = B_0 \text{ T}. \tag{4.6}$$

A magnetic field profile of the field map and the old and new hard-edge model can be seen in Fig.4.3.

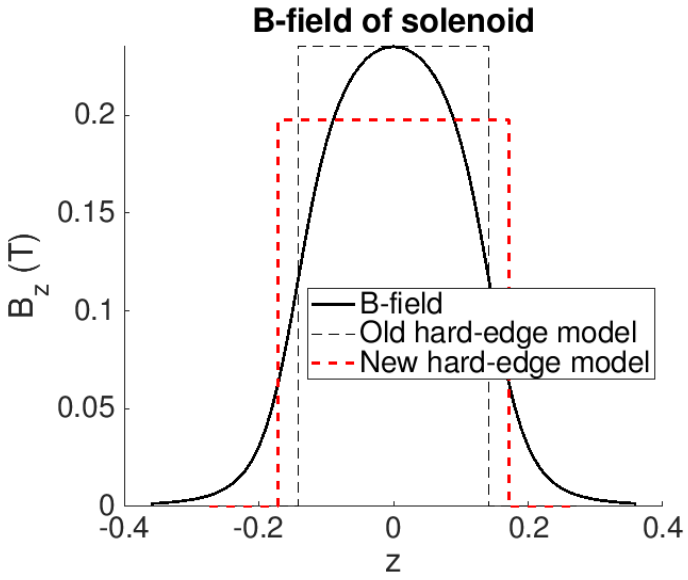

Figure 4.3: Magnetic field of solenoid for a peak field strength of 235 mT, together with its old and new hard-edge model.

A fixed length and a linear dependent B-field gives a new hard-edge model just as simple as the old, but with a higher accuracy for the LEBT solenoids. This can be seen in a beam centroid trajectory example through the LEBT for the field map, the old and the new hard-edge model in Fig. 4.4. As can be seen in this figure, the old hard-edge model has a stronger focusing than the new hard-edge model.

An error estimation was done for a simulation though the solenoid for different field strengths, and for two different realistic initial offsets of $x, y = 0.1$ mm and $x', y' = 0.1$ mrad, and $x, y = 0.4$ mm and $x', y' = 0.4$ mrad. The estimated errors can be seen in Fig. 4.5. The errors, ϵ, were calculated as,

$$\epsilon_{r,\%} = 100 \cdot \left| \frac{\epsilon_{r,\text{mm}}}{r_{\text{field map}}} \right|, \qquad \epsilon_{r,\text{mm}} = \left| r_{\text{hard-edge}} - r_{\text{field map}} \right|, \tag{4.7}$$
$$\epsilon_{r',\%} = 100 \cdot \left| \frac{\epsilon_{r',\text{mm}}}{r'_{\text{field map}}} \right|, \qquad \epsilon_{r',\text{mm}} = \left| r'_{\text{hard-edge}} - r'_{\text{field map}} \right|, \tag{4.8}$$
$$\epsilon_{\Phi,\%} = 100 \cdot \left| \frac{\epsilon_{\phi,\text{rad}}}{2\pi} \right|, \qquad \epsilon_{\Phi,\text{mm}} = \left| \Phi_{\text{hard-edge}} - \Phi_{\text{field map}} \right|, \tag{4.9}$$

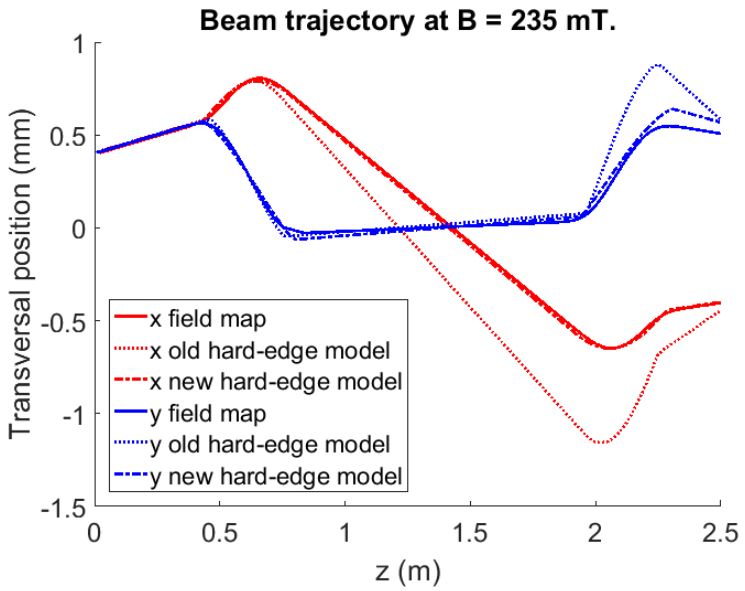

Figure 4.4: Centroid trajectory through the LEBT for a beam with initial conditions $x, y = 0.4$ mm and $x', y' = 0.4$ mrad. The two solenoids are centered at $z = 0.6$ m and $z = 2.1$ m and has a peak field of 235 mT.

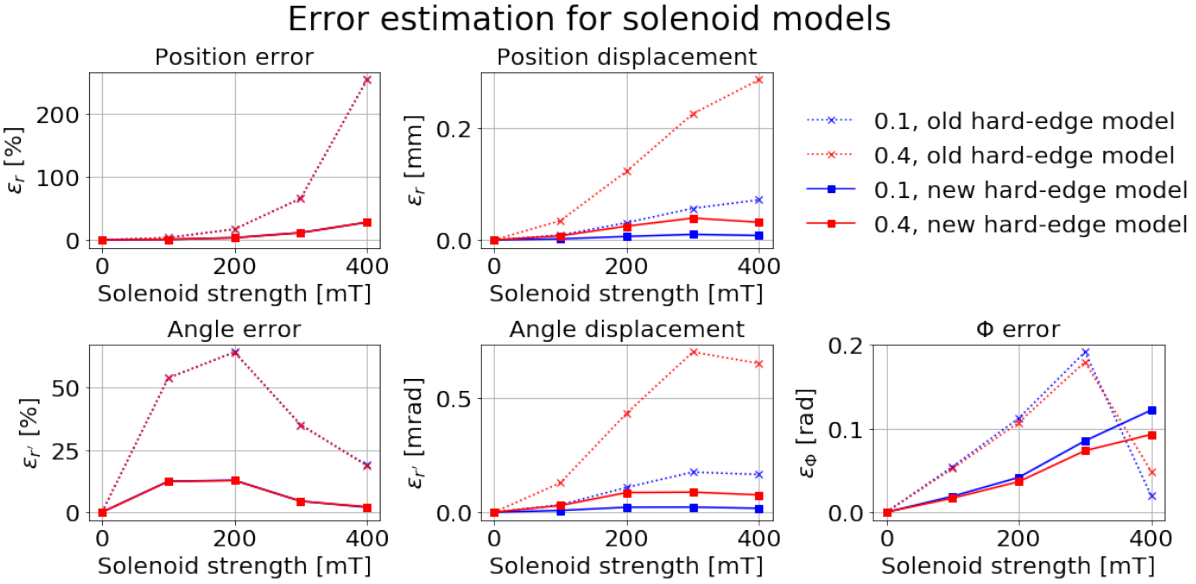

Figure 4.5: Solenoid positional, angular and rotational errors for an incoming beam of two different offsets: $x, y = 0.1$ mm and $x', y' = 0.1$ mrad, and $x, y = 0.4$ mm and $x', y' = 0.4$ mrad.

where,

$$r = \sqrt{x^2 + y^2}, \qquad \Phi = \arg(x + iy) \tag{4.10}$$

The position error for a solenoid of 200 mT was reduced from 17.0% to 3.4%, while the angle error was reduced from 64.0% to 12.7%. The increase of the percentage error as the solenoid reaches 400 mT is due to the fact that the output position of the beam is close to the origin, which is creating a large percentage error for the models.

During the time of this work, the Integrated Control System section of ESS successfully developed OpenXAL to be able to include the solenoids as field maps. Therefore, the continuous use of the reference work with the solenoids will be as field maps.

4.3 Steerers in the thin lens approximation

There are four steerers in the LEBT. The steerers are positioned inside the solenoids, with one vertical (referred to as V-steerer) and one horizontal (referred to as H-steerer) for each of the two solenoids. Reference field maps could be produced for TraceWin from field measurements, see Fig. 4.6, where the H-steerer, as it is positioned on top of the V-steerer, produces a slightly lower peak field.

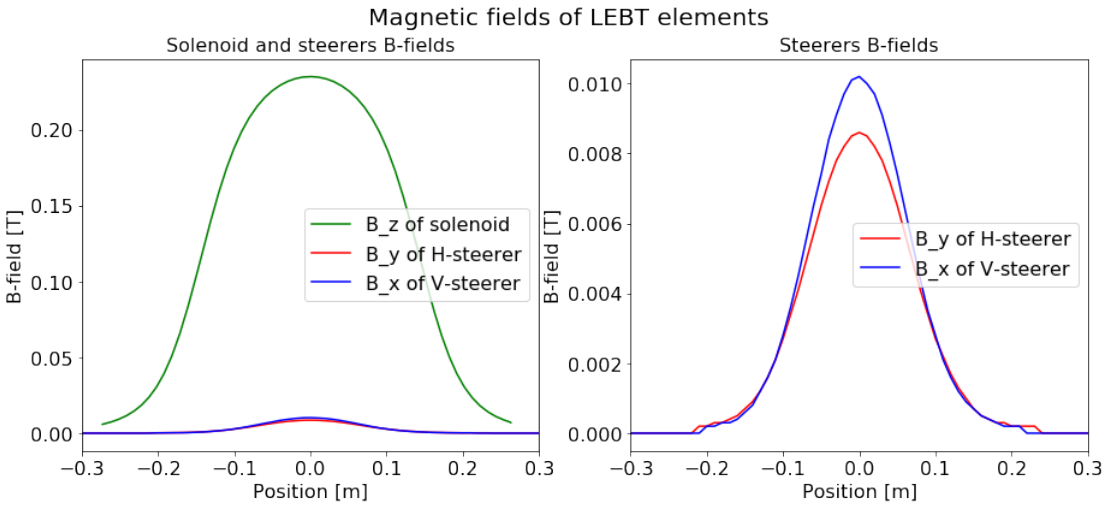

Figure 4.6: B-fields of realistic strengths for (left) solenoid with steerers and (right) steerers only.

The first attempt was done by modeling the steerers with the thin lens approximation, where the total angular kick is concentrated at one single point: the centre of the element. This approximation would be highly desirable, since the resulting beam trajectory for a beam given a single kick at the centre of the beam-rotating solenoid can be easily implemented, which would be beneficial for the LEBT application.

The magnetic integrals for the horizontal and vertical steerer, $(BL)_h$ and $(BL)_v$, were calculated as,

$$(BL)_h = \int_{-\infty}^{\infty} B_y(z)dz, \qquad (BL)_v = \int_{-\infty}^{\infty} B_x(z)dz, \tag{4.11}$$

where $B_y(z)$ is the B-field of the horizontal steerer and $B_x(z)$ is the B-field of the vertical steerer. These magnetic integrals convert to an angular kick, dx' and dy' accordingly with (2.51).

A simulation for a beam trajectory through the thin lens approximation, compared to a field map simulation with and without a solenoid can be seen in Fig. 4.7. Without the solenoid, the steerers were accurately expressed by the thin lens approximation. With a solenoid though, the model lost its accuracy, which shows that the width of the steerer's B-field is non-negligible for a solenoid of a strong realistic strength of 400 mT. The outgoing beam through the thin lens approximation reached an angle error of 11.5% for the H-steerer and 9.8% for the V-steerer, calculated for $r' = \sqrt{x'^2 + y'^2}$ as,

$$\epsilon_{\%} = 100 \cdot \left| \frac{r'_{\text{thin lens}} - r'_{\text{field map}}}{r'_{\text{field map}}} \right|. \tag{4.12}$$

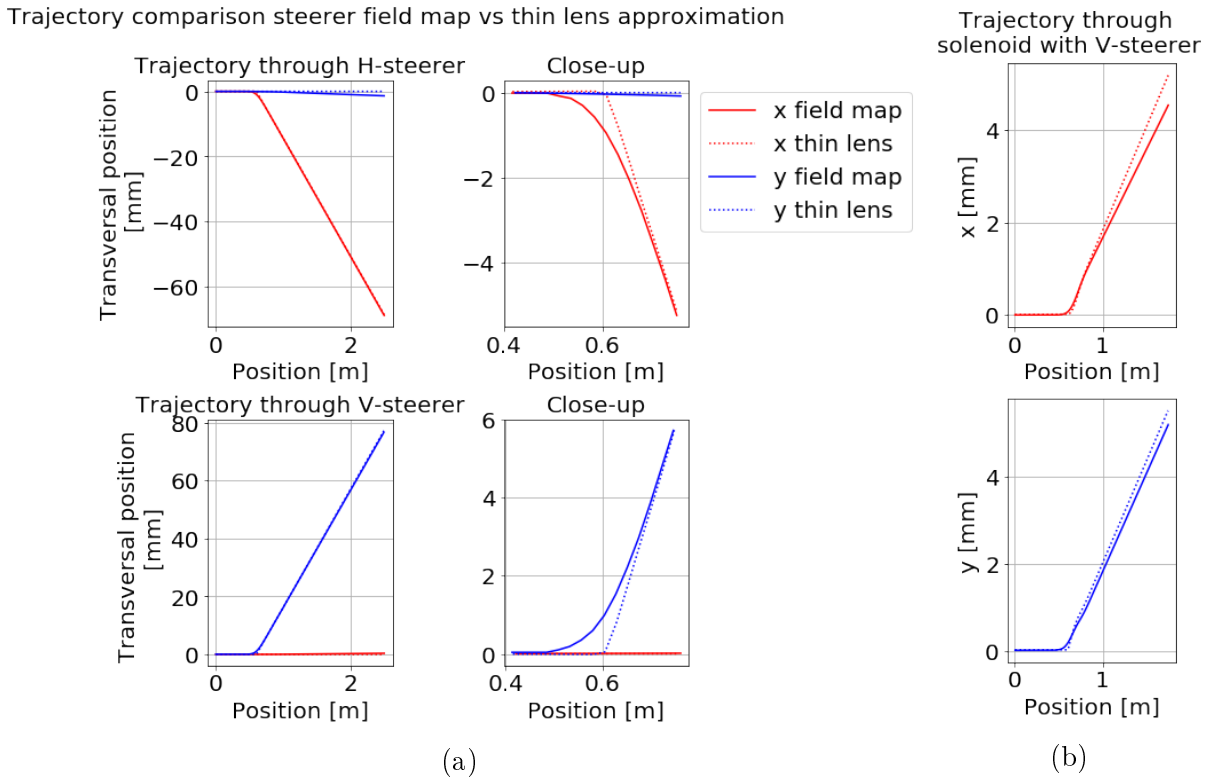

(a) (b)

Figure 4.7: Trajectory of a beam through the thin lens approximation and field map for a strong H- and V-steerer of a peak field 8.6 mT and 10.3 mT respectively, (a) without solenoid and (b) with a strong solenoid of peak field 400 mT.

To affect the beam at different stages of its rotation within the solenoid, a further modelling attempt was made for the V-steerer by expressing it as three thin lenses, positioned in the centre, $P2 = 0$, and at the half maxima of the steerer's B-field, located at $P1 = -0.0734$ and $P3 = 0.0734$ (see Fig. 4.8). To calculate the magnetic integral, the B-field was divided into three segments, 1, 2 and 3, with an integral of,

$$BL_{v,1} = \int_{-\infty}^{-\mathrm{D}} B_x(z)dz, \quad BL_{v,2} = \int_{-\mathrm{D}}^{\mathrm{D}} B_x(z)dz, \quad \text{and} \quad BL_{v,3} = \int_{\mathrm{D}}^{\infty} B_x(z)dz, \tag{4.13}$$

where D is the integration divider seen in Fig. 4.8. The position of D was calculated from the constraint that the positions of P1 and P3 must be balanced by an equal magnetic

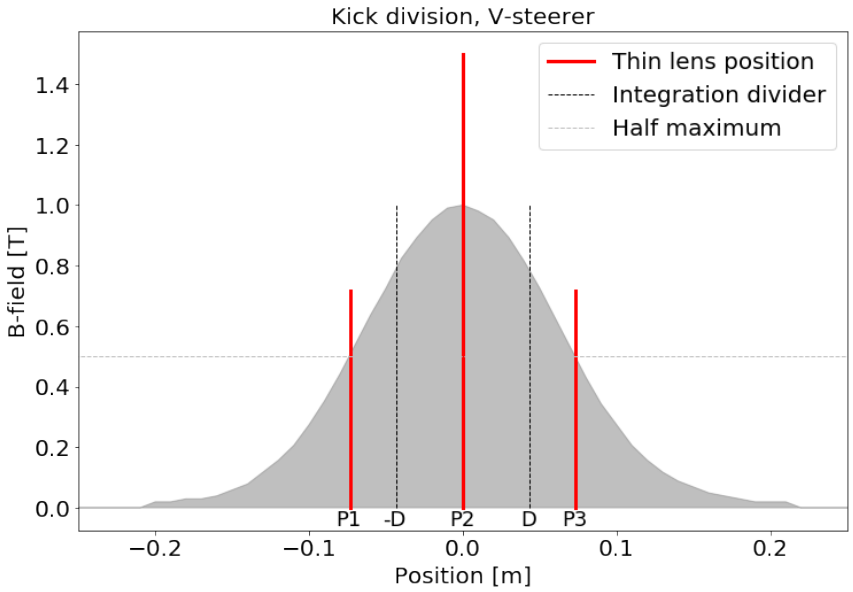

Figure 4.8: Position of thin lenses for the three-lens approximation of the V-steerer.

integral from both sides of the kick, i.e. from,

$$\int_{-\infty}^{\mathrm{P1}} B_x(z)dz = \int_{\mathrm{P1}}^{-\mathrm{D}} B_x(z)dz,$$

and also,

$$\int_{\mathrm{D}}^{\mathrm{P3}} B_x(z)dz = \int_{\mathrm{P3}}^{\infty} B_x(z)dz.$$

With the calculated integration divider positioned at $D = \pm 0.0435$, the magnetic integral ratios could be calculated from a normalized B-field to be,

$$BL_{v,1} = 0.0386 \cdot B_{x,\mathrm{peak}}, \quad BL_{v,2} = 0.0805 \cdot B_{x,\mathrm{peak}}, \quad BL_{v,3} = 0.0386 \cdot B_{x,\mathrm{peak}}. \tag{4.14}$$

With the same procedure, the magnetic integral ratios of the H-steerer were calculated to be,

$$BL_{h,1} = 0.0411 \cdot B_{y,\mathrm{peak}}, \quad BL_{h,2} = 0.0854 \cdot B_{y,\mathrm{peak}}, \quad BL_{h,3} = 0.0411 \cdot B_{y,\mathrm{peak}}. \tag{4.15}$$

A simulation was done for this "three-lenses approximation" for both the V-steerer and the H-steerer. The three-lenses approximation reduced the angle error from 11.5% to 4.5% for the H-steerer and from 9.8% to 3.7% for the V-steerer for the maximum current configuration. Note that these errors are for the worst case scenario (maximum B-field). This accuracy was considered acceptable, and the three-lenses approximation was then implemented into OpenXAL. Still, a model with five kicks was developed for scientific curiosity.

In the five lenses approximation, the thin lenses were positioned at the centre of the field, and at 1/4 and 3/4 of the peak field, see Fig. 4.9. This division, that followed the same procedure as the three lens approximation, gave the magnetic integral ratios,

$$BL_{v,1} = 0.0163 \cdot B_{x,\mathrm{peak}}, \quad BL_{v,2} = 0.0384 \cdot B_{x,\mathrm{peak}}, \quad BL_{v,3} = 0.0483 \cdot B_{x,\mathrm{peak}}, \tag{4.16}$$

$$BL_{v,4} = 0.0384 \cdot B_{x,\mathrm{peak}}, \quad BL_{v,5} = 0.0163 \cdot B_{x,\mathrm{peak}}, \tag{4.17}$$

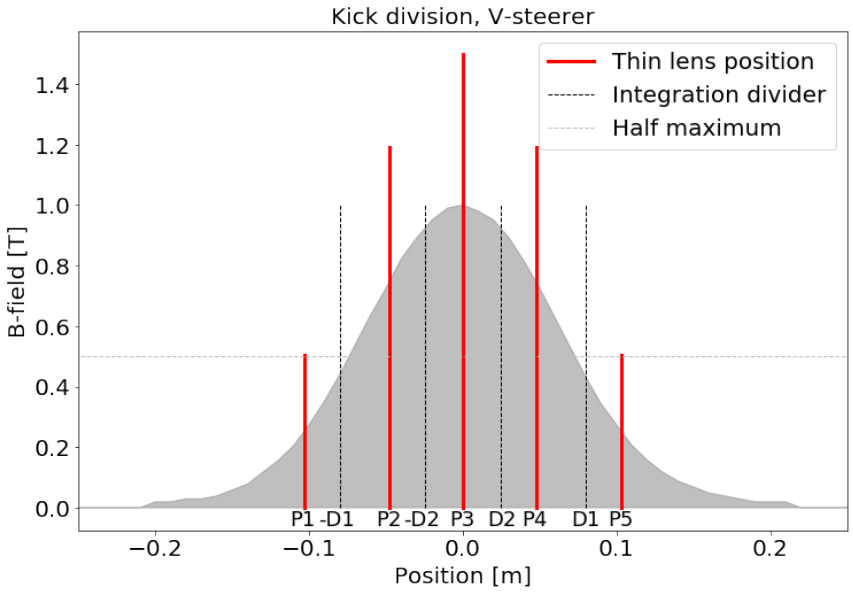

Figure 4.9: Position of thin lenses for the five-lens approximation of the V-steerer.

and

$$BL_{h,1} = 0.0176 \cdot B_{y,\text{peak}}, \quad BL_{h,2} = 0.0405 \cdot B_{y,\text{peak}}, \quad BL_{h,3} = 0.0515 \cdot B_{y,\text{peak}}, \tag{4.18}$$

$$BL_{h,4} = 0.0405 \cdot B_{y,\text{peak}}, \quad BL_{h,5} = 0.0176 \cdot B_{y,\text{peak}}. \tag{4.19}$$

This reduced the error to 2.6% for the H-steerer and to 2.0% for the V-steerer.

An error estimation of the three different models for steerers of various strengths and through a solenoid with field from 0 to 400 mT can be seen Fig. 4.10.

4.4 Beam envelope evolution

The evolution of the beam's RMS-size, σ, can be calculated by OpenXAL. Unfortunately, OpenXAL is only designed to work with a bunched probe. The LEBT is the only section in the ESS linac where the beam is not bunched, but rather continuous, since it is the first section after the proton extraction.

The envelope dynamics of a bunched beam and a continuous beam differ when space charge is present. In the LEBT, the energy is not on a relativistic level, which means that the space charge has a strong impact on the beam. Without a continuous beam option, a bunched beam can be manipulated to resemble the behaviour of a continuous beam, where once again TraceWin was used for benchmarking.

The difference of the resulting space charge force between a bunched and continuous beam can be compared with electrodynamics. A bunch charge will be surrounded by a spherical radial electric field, which results in an envelope evolution in a spherically radial manner, while for an infinitely long string of charge, the longitudinal net force will sum to zero [7].

A first attempt to resemble the behaviour of a continuous beam was made by simply increasing the initial longitudinal emittance by 500%, so that $\sigma_z \gg \sigma_x, \sigma_y$. This attempt reduced the longitudinal RMS increase from 90% to 5.8% throughout the LEBT, indicating a lower space charge force in the longitudinal direction. However, this attempt only increased the transverse error of the envelope when compared to TraceWin. The next

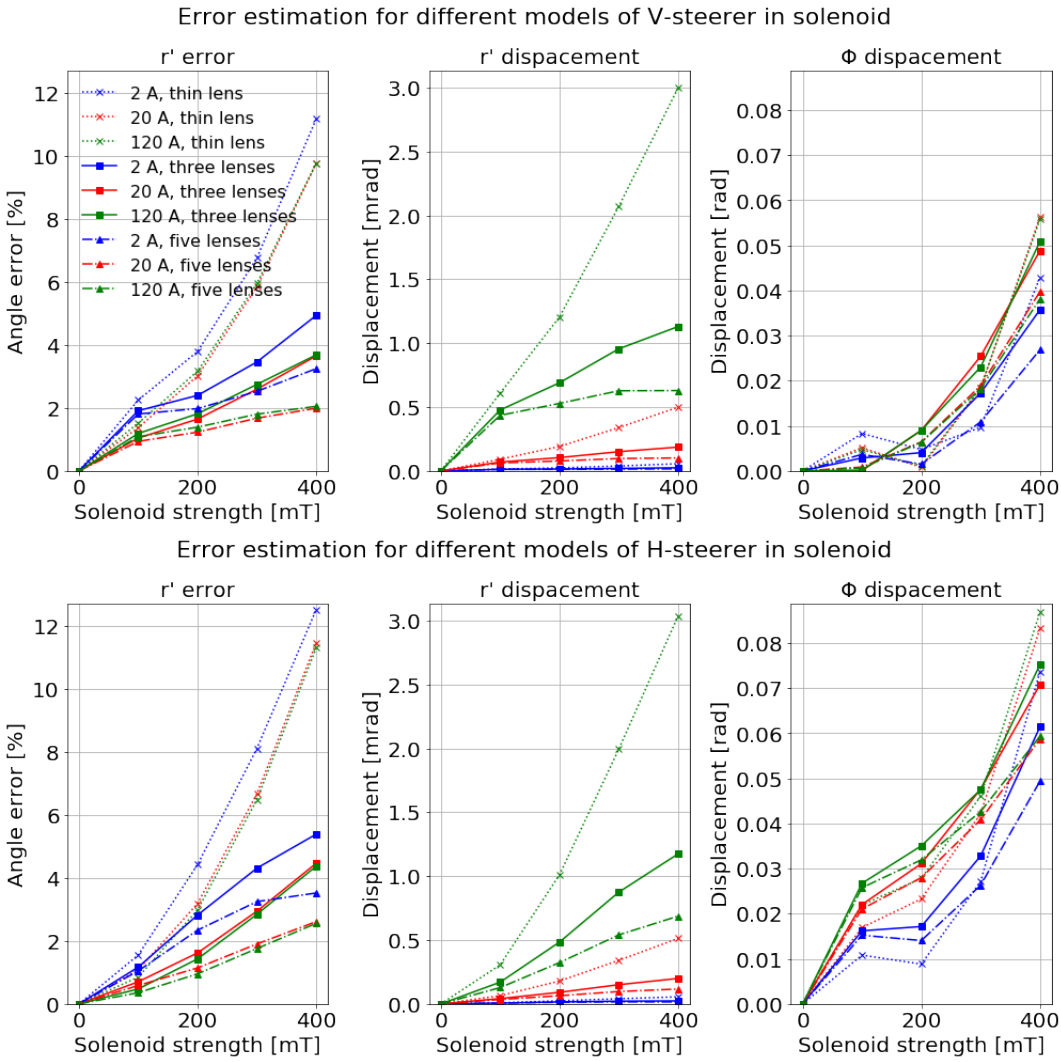

Figure 4.10: Error of horizontal and vertical steerer modelled by the thin lens, three-lenses and five-lenses approximation.

step was then done by comparing the space charge force algorithms for a bunched and continuous beam.

The acceleration from the space charge for a continuous beam is [12],

$$x'' = \frac{2K}{a_x(a_x + a_y)} \cdot x \qquad\qquad y'' = \frac{2K}{a_y(a_x + a_y)} \cdot y, \tag{4.20}$$

where

$$K = \frac{|q| \cdot I}{\pi \epsilon_0 m c^3 \beta_r^3 \gamma_r^3},$$

is the beam generalized perveance, a_x, a_y are the semi-axes of the homogeneous ellipse (2 times the RMS beam sizes), I is the average beam current, and ϵ_0 is the vacuum permittivity. These equations were matched with the space-charge algorithm for a bunched beam,

$$w'' = \frac{K_w}{a_x^* a_y^* a_z^*} \cdot w^*, \tag{4.21}$$

with

$$K_w = \frac{3 \cdot |q| \cdot Q}{4\pi \epsilon_0 m c^2 \beta_r^2 \gamma_r^2} \cdot f_w(a_x^*, a_x^*, a_y^*)$$

and,

$$f_w(a_x^*, a_y^*, a_z^*) = \int_0^\infty \frac{ds}{(a_w^{*2} + s)\sqrt{(a_x^{*2} + s)(a_y^{*2} + s)(a_z^{*2} + s)}},$$
$$f_x + f_y + f_z = 1,$$

where w is the chosen axis, Q is the bunch charge, a_x^*, a_y^* and a_z^* are the beam semi-axes of a uniform ellipsoid ($\sqrt{5}$ times the RMS beam size) in the beam frame, so that $a_w^* = \gamma_r a_w$. In the LEBT, $\gamma_r \approx 1$.

In order to have the same defocusing force, a current ratio between the continuous and manipulated bunched beam could be calculated for the chosen longitudinal emittance,

$$I_\mathrm{b} = 22.703 \cdot I_\mathrm{c}, \tag{4.22}$$

where I_b is the modified bunched beam current and I_c is the current of the continuous beam. This ratio, together with the altered emittance $\varepsilon_z = 0.547588\ \pi$.mm.mrad, reduced the estimated envelope error at the entrance of the RFQ from an initial value of 41.8% to 11.5%. At this entrance, the beam is very focused, and space charge is higher, which creates this peak error for the modified beam (see Fig. 4.11). The average error throughout the LEBT is 1.9%. These errors was calculated for a beam current of 74 mA and a space charge compensation of 95% through the LEBT as,

$$\epsilon_\mathrm{mm} = |\sigma_{\text{ mod}} - \sigma_{\text{ field map}}|, \qquad \epsilon_\% = 100 \cdot \frac{|\sigma_{\text{ mod}} - \sigma_{x,y\text{ field map}}|}{\sigma_{\text{ field map}}}, \tag{4.23}$$

where $\sigma_x = \sigma_y = \sigma$. The error throughout the LEBT can be seen as a plot in Fig. 4.11. An example of the envelope evolution for the continuous and manipulated bunched beam can be seen in fig 4.12.

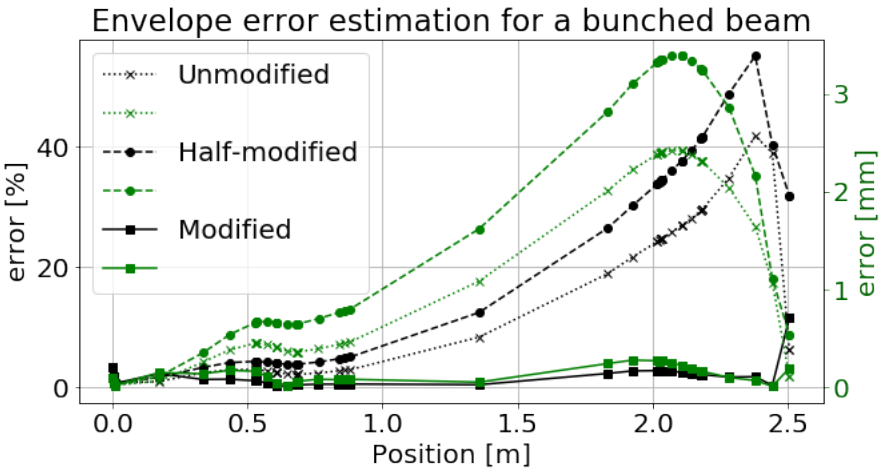

Figure 4.11: Envelope error through the LEBT with two active solenoids with a typical peak field of 235 mT for the unmodified bunched beam, half-modified bunched beam with an increased longitudinal emittance, and the fully modified bunched beam with increased longitudinal emittance and rescaled current. Initial conditions are presented in Table 2.1.

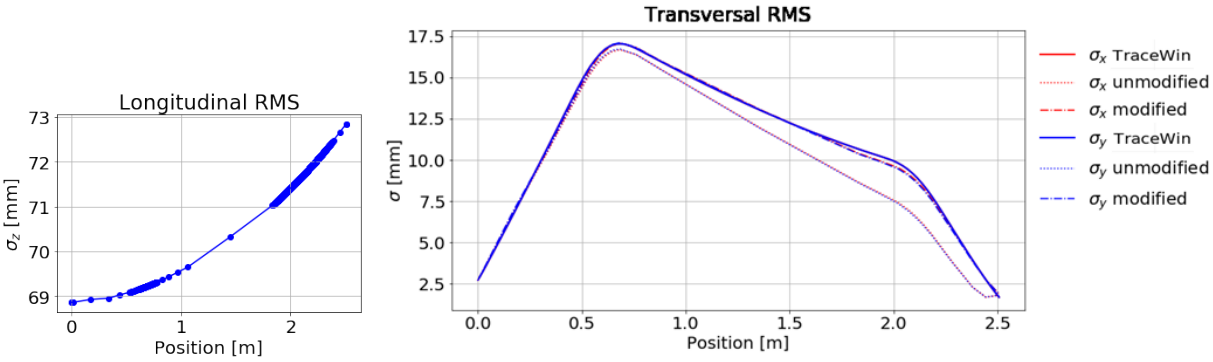

(a) (b)

Figure 4.12: Envelope dynamics through the LEBT with two active solenoids with a typical peak field of 235 mT. Initial conditions are presented in Table 2.1.(a) Longitudinal RMS for a modified bunched beam.(b) Transverse RMS for a continuous and modified bunched beam.

4.5 LEBT Application Program Interface (API)

For the commissioning and maintenance of the LEBT, the elements will be managed from the control room. The elements might have to be modified daily due to changes of the beam, or in best case, only when the ion source is modified. For this to run as smoothly as possible, a user-friendly program is needed which includes trajectory and envelope simulation for different element and beam parameters. In this thesis, a simple user-interface was created with fixed parameters for the initial emittance and space charge compensation, and with editable parameters for the beam offset and element parameters for the models derived in the previous sections.

The implementation of the newly derived models in OpenXAL, that was initially written in Python, was now transferred to a Java program. Code was written so that after a run, a variety of data could be retrieved, from which plots could be produced. An API was created, and in the resulting application, the initial phase space vector (x, x', y, y') can be set as well as the beam current. The elements' currents can be set as well, which are relative to the magnetic peak fields accordingly with Table 4.1.

Parameter	**Ratio**
$B_{\text{sol,peak}}/I_{\text{sol}}$	$8.1531 \cdot 10^{-4}$
$B_{h,\text{peak}}/I_h$	$7.1667 \cdot 10^{-5}$
$B_{v,\text{peak}}/I_v$	$8.5833 \cdot 10^{-5}$

Table 4.1: Current-to-magnetic field ratios for the LEBT solenoids, horizontal and vertical steerers.

When the simulation is run by clicking Run!,a trajectory plot and an envelope plot are displayed, see Fig. 4.13. The coordinate system can be changed from Cartesian to cylindrical, that is calculated according to (4.10). The envelope can be scaled as nσ, where n is an integer. In the envelope plot, the centroid offset can be either included or excluded, where an included offset in the cylindrical coordinate system is the optimal view to see if the beam stays within the LEBT vacuum chamber or not. In Fig. 4.13, the chamber which is plotted in black and the envelope in colour, see Fig. 4.13.

Figure 4.13: Application for trajectory and envelope simulation in the LEBT.

Chapter 5

Discussion and outlook

The LEBT is the first of all sections of the ESS linac to be commissioned, which is planned to be executed in the spring of 2018. A complete linac is expected to be ready in 2021, after the commissioning of all the following sections. The proton beam will then be ready to collide with the tungsten target and produce neutrons.

The produced neutrons will be used to probe materials on the molecular level, everything from motors and medicine, to plastics and proteins. Detailed studies are dependent on how many neutrons can be produced by a neutron source, and ESS will provide up to 100 times brighter neutron beams than existing facilities today [26]. ESS is important for the development of new and better computer chips, cosmetics, detergents, textiles, paints, fuels, drugs, batteries and plastics. Industrial drivers such as fuel cells, superconductors, innovative structural engineering, climate, transportation and food technologies, pharmaceuticals, medical devices and clean energy, are all dependent on advances in the capacity and capability of the science of neutron scattering. Research with neutrons will finally give knowledge that improves our everyday lives, our health and the environment. ESS is positioned as the vanguard of the next century of experimental science and is the world's next great Big Science facility.

As the commissioning of the LEBT approaches, a tool to be used in the control room to characterize and test the beam parameters is needed. In this thesis, models for the solenoid and steerers were tested and improved. The position error for a solenoid of 200 mT was reduced from 17.0% to 3.4%, while the angle error was reduced from 64.0% to 12.7%. The worst case angle error of the horizontal steerer was reduced from 11.5% to 4.5% and the vertical steerer from 9.8% to 3.7%. Also, an accurate calculation of the envelope evolution along the low energy section was successfully achieved by rescaling the longitudinal beam size and total beam current. The steerer and envelope models were then implemented in OpenXAL and a first draft of the LEBT application was completed, which can be used in the control room to simulate the trajectory and envelope evolution in the LEBT for different beam offsets and element strengths.

Even though the improved hard-edge model for the solenoid is not used in the final application, it can still be beneficial for the scientists in the control room. For instance, if a specific beam rotation is desired, calculations can easily be done with this model to estimate the necessary magnetic field.

Although the modification of the longitudinal emittance and total current, that was in OpenXAL to simulate a continuous beam, results in good values of RMS beam size along the LEBT, it would be preferable if the beam dynamics for a continuous beam would be implemented in OpenXAL, so that the initial parameters of the real machine could be

used.

The LEBT application will be further developed by the Beam Physics section of ESS, and will finally be used in the control room during commissioning and routine operations of the LEBT. Editable parameters that will be added include emittance and Twiss parameters for the input beam, level of space charge compensation and also parameters for other elements in the LEBT, such as chopper voltage and iris radius. As the LEBT is being commissioned, the application will be used firstly to estimate the beam parameters together with the NPMs with trial-and-error simulations, and lastly to simulate the optimal element parameters, that will result in a focused beam travelling straight into the RFQ.

The final work of this thesis resulted in a conference paper, that will be presented at the International Particle Accelerator Conference (IPAC'18) in Vancouver in the spring of 2018. The abstract and title of the paper can be found in Appendix III.

Acknowledgements

First and foremost, I would like to thank Natalia Milas, who has been an amazing supervisor and friend. My calm and confidence, that I have felt surprised of having during these important months, no doubt has their foundation in Natalia's excellent guidance and support, for everything from physics and programming to knitting and life skills.

I would also like to thank Mamad Eshraqi, first of all for receiving me as his master student, and also for making sure that I quickly felt like part of the group, and for always asking me how I'm doing. His great sense of humour has constantly given me a lot of laughs.

I also would like to thank the other scientists of the Beam Physics section: Ryoichi Miyamoto for his dedication and patience during my endless questions about emittance, Ciprian Plostinar for stories, laughter and for being such a great go-kart driver, Mark Munos for being an awesome office mate, Yngve Levinsen and Øystein Midttun for Norway stories, and Renato de Prisco for letting me steal his office.

I would like to thank great lunch break comrades: Juan Esteban Müller for help and support in programming and for constantly being astonished by the amount of food on my plate, Emanuele Laface for teaching me about symplectic integrators and for ordering my latte macchiatos, Ben Folsom for great company at the yarn-store visits, and Håkan Danered for interesting discussions.

I would also like to thank all the people of ESS that have enlightened by stay: Saeid Pirani, Andreas Jansson, Caroline Prabert, Lali Tchelidze, Tom Shea and all the rest.

During this thesis work, I also got married. I would like to thank my wife Maïté Louisy, whose love, understanding and support have been absolutely vital for my happiness and well-being during this time.

Bibliography

[1] M. Åberg, N. Ahlfors, R. Ainsworth, C. Alba-Simionesco, S. Alimov, N. Aliouane, B. Alling, K. G. Andersson, N. H. Andersen, B. R. Hansen, *et al.*, *ESS technical design report*. European Spallation Source, 2013.

[2] C. Plostinar. Personal communication, 2017.

[3] O. Midttun. Personal communication, 2017.

[4] A. Letchford, "Beam dynamics in linacs."

[5] O. Midttun, L. Celona, B. Cheymol, R. Miyamoto, L. Neri, and C. Thomas, "Measurements and simulations of the beam extraction from the ess proton source,"

[6] I. S. Grant and W. R. Phillips, *Electromagnetism*. John Wiley & Sons, 2013.

[7] H. Benson, *University physics*. John Wiley & Sons, 2008.

[8] J. Rosenzweig, *Fundamentals of beam physics*. Oxford University Press Oxford, 2003.

[9] J. R. Taylor, *Classical mechanics*. University Science Books, 2005.

[10] R. Miyamoto, *Diagnostics of the Fermilab Tevatron using an AC dipole*. The University of Texas at Austin, 2008.

[11] H. Wiedemann, *Particle accelerator physics*. Springer, 2015.

[12] T. P. Wangler, *RF Linear accelerators*. John Wiley & Sons, 2008.

[13] A. J. Dragt, R. L. Gluckstern, F. Neri, and G. Rangarajan, "Theory of emittance invariants," in *Frontiers of Particle Beams; Observation, Diagnosis and Correction*, pp. 94–121, Springer, 1989.

[14] H. J. Müller-Kirsten, *Basics of statistical physics*. World Scientific, 2013.

[15] C. K. Allen and N. Pattengale, "Theory and technique of beam envelope simulation," *Los Alamos National Laboratory Internal Report LA-UR-02-4979*, 2002.

[16] A. W. Chao, K. H. Mess, M. Tigner, and F. Zimmermann, *Handbook of accelerator physics and engineering*. World Scientific, 1999.

[17] T. L. Chow, *Introduction to electromagnetic theory: a modern perspective*. Jones & Bartlett Learning, 2006.

[18] M. Conte and W. W. MacKay, *An introduction to the physics of particle accelerators*. world scientific, 2008.

[19] "Ess-0094638." ESS internal document, 2017.

[20] D. Uriot and N. Pichoff, "Tracewin," *CEA Saclay, June*, 2014.

[21] I. Pelaia *et al.*, "Open xal build system," 2015.

[22] G. Van Rossum *et al.*, "Python programming language.," in *USENIX Annual Technical Conference*, vol. 41, p. 36, 2007.

[23] H. Schildt, *Introducing JavaFX 8 Programming*. McGraw-Hill Education, 2015.

[24] M. Taman, *JavaFX Essentials*. Packt Publishing Ltd, 2015.

[25] S. Bernal, H. Li, R. Kishek, B. Quinn, M. Walter, M. Reiser, P. O'Shea, and C. Allen, "Rms envelope matching of electron beams from "zero" current to extreme space charge in a fixed lattice of short magnets," *Physical Review Special Topics-Accelerators and Beams*, vol. 9, no. 6, p. 064202, 2006.

[26] E. P. Sciences and E. S. W. G. N. L. Group, *Neutron scattering facilities in Europe: Present status and future perspectives*. Dipartimento di Fisica - Università degli Studi di Milano, 2016.

Appendix I - Code: Trajectory simulation in Python

The code presented below is a simulation of the beam trajectory within the LEBT. The solenoids are modelled by the new hard-edge model presented in Chapter 4, while the steerers (correctors) are represented by the thin lens approximation described in Section 2.3.2. A simulation produced by this code can be seen in Fig. 5.1

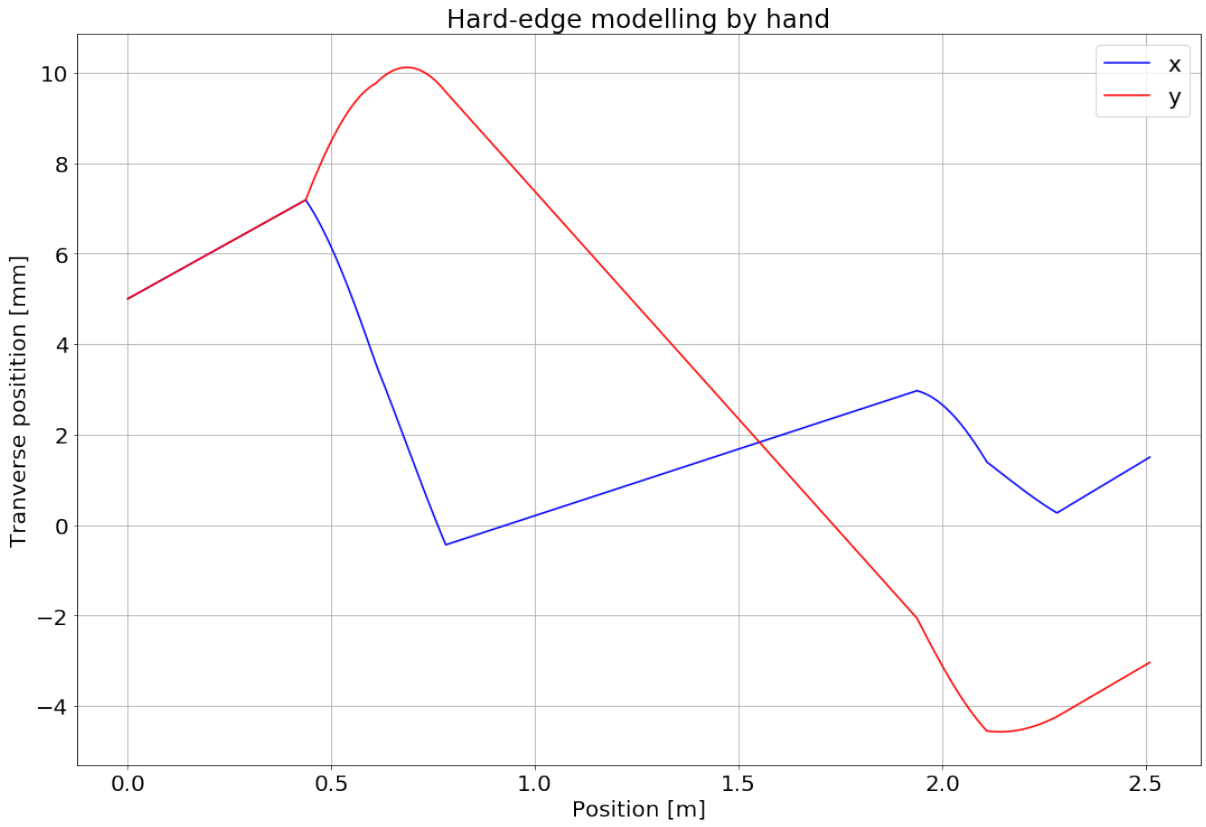

Figure 5.1: Plotting result from simulation of above code.

```
import matplotlib.pyplot as plt
%matplotlib inline
import numpy
import math
import scipy.linalg
from sympy import *
```

Listing 5.1: Imports

```
#----------Adjustable parameters
#Initial conditions
x = 0.005
x_ = 0.005
y = 0.005
y_ = 0.005

#Steerers
H1_B_max = -0.001
H2_B_max = -0.002

V1_B_max = 0.001
V2_B_max = 0.002

#Solenoids
sol1_B_max = 0.235
sol2_B_max = 0.235
#-------------------------------

#Proton properties in SI units
m = 1.6726219*10**(-27);
q = 1.6021766208*10**(-19);
E = 75*10**3*q;
c = 2.99797458*10**8;
gamma = E/(m*c**2)+1;
betagamma = sqrt(gamma**2 - 1);
Er = m*c**2 #rest energy

#Solenoids
const_s = q/(2*m*c*betagamma);

#Sol1
sol1_eff_len = 0.3427
sol1_eff_B = 0.8524*sol1_B_max
sol1_k = sol1_eff_B*const_s

#Sol2
sol2_eff_len = 0.3427
sol2_eff_B = 0.8524*sol2_B_max
sol2_k = sol2_eff_B*const_s

#Steerers (hor or vert)
const_k = q*c/(Er*betagamma)

V1_BL = 0.15765*V1_B_max
V2_BL = 0.15765*V2_B_max

H1_BL = 0.16765*H1_B_max
H2_BL = 0.16765*H2_B_max

V1kick_dp_x = const_k*V1_BL
V2kick_dp_x = const_k*V2_BL

H1kick_dp_y = -const_k*H1_BL
H2kick_dp_y = -const_k*H2_BL

#Drift to solenoid
pre_len = 0.6081-sol1_eff_len/2
```

```

#Drift between solenoids
middle_len = 1.4988-sol1_eff_len/2-sol2_eff_len/2

#Drift after solenoid
post_len = 0.399-sol2_eff_len/2
```

Listing 5.2: Parameter settings

```
def M_drift(d):
  return Matrix([[1,d,0,0,0],
                 [0,1,0,0,0],
                 [0,0,1,d,0],
                 [0,0,0,1,0],
                 [0,0,0,0,1]])

def M_kick(dp_x,dp_y,l=1):
  return Matrix([[1,0,0,0,0],
                 [0,1,0,0,dp_x*l],
                 [0,0,1,0,0],
                 [0,0,0,1,dp_y*l],
                 [0,0,0,0,1]])

def M_sol(k,l):
  s = sin(k*l)
  c = cos(k*l)
  if k != 0:
    return Matrix([[c**2,s*c/k,s*c,s**2/k,0],
                   [-k*s*c,c**2,-k*s**2,s*c,0],
                   [-s*c,-s**2/k,c**2,s*c/k,0],
                   [k*s**2,-s*c,-k*s*c,c**2,0],
                   [0,0,0,0,1]])
  else:
    return Matrix([[1,l,0,0,0],
                   [0,1,0,0,0],
                   [0,0,1,l,0],
                   [0,0,0,1,0],
                   [0,0,0,0,1]])
```

Listing 5.3: Transfer matrices

```
In = Matrix([[x],[x_],[y],[y_],[1]])

#Simulation variables
dz = 0.001
z_list = [0]
z = 0
pos = In
pos_list = [In]

while z < pre_len:
  z+=dz
  z_list.append(z)
  pos = M_drift(dz)*pos
  pos_list.append(pos)

#Going through half solenoid_!
now = z
while z < now+sol1_eff_len/2:
```

```
  z+=dz
  z_list.append(z)
  pos = M_sol(sol1_k,dz)*pos
  pos_list.append(pos)

#Corrector_1
pos = M_kick(V1kick_dp_x,H1kick_dp_y)*pos

#Going through half solenoid_1
now = z
while z < now+sol1_eff_len/2:
  z+=dz
  z_list.append(z)
  pos = M_sol(sol1_k,dz)*pos
  pos_list.append(pos)

#Drift between solenoids
now = z
while z < now+middle_len:
  z+=dz
  z_list.append(z)
  pos = M_drift(dz)*pos
  pos_list.append(pos)

#Going through half solenoid body_2
now = z
while z < now+sol2_eff_len/2:
  z+=dz
  z_list.append(z)
  pos = M_sol(sol2_k,dz)*pos
  pos_list.append(pos)

#Corrector_2
pos = M_kick(V2kick_dp_x,H2kick_dp_y)*pos

#Going through half solenoid_2 body
now = z
while z < now+sol2_eff_len/2:
  z+=dz
  z_list.append(z)
  pos = M_sol(sol2_k,dz)*pos
  pos_list.append(pos)

#Drift in collimator
now = z
while z < now+post_len:
  z+=dz
  z_list.append(z)
  pos = M_drift(dz)*pos
  pos_list.append(pos)

#creating the x_list
x_list = []
i = 0
while i < len(pos_list):
  x_list.append(pos_list[i][0]*1.0e+3)
  i+=1

```

```
#creating the y_list
y_list = []
i = 0
while i < len(pos_list):
  y_list.append(pos_list[i][2]*1.0e+3)
  i+=1
```

Listing 5.4: Simulation

```
fig, (ax1) = subplots(ncols=1, nrows=1, figsize=(18,12))

ax1.set_xlabel('Position [m]')
ax1.set_ylabel('Tranverse posititon [mm]')

ax1.plot(z_list,x_list,'-b',label = 'x')
ax1.plot(z_list,y_list,'-r',label = 'y')
ax1.set_title('Hard-edge modelling by hand')

ax1.legend()
ax1.grid()

show()
```

Listing 5.5: Plotting

Appendix II - Code: Transfer matrix from field map segmentation

The magnetic field profile can be divided into segments to produce a more accurate transfer matrix, see Fig. 4.1. The code that calculates this matrix is presented below. With this code, the transfer matrix of a segmented field map for a solenoid of 235 mT was calculated to be:

$$M_{\text{sol, 235}} = \begin{pmatrix} 0.3339 & 0.2705 & 0.3818 & 0.3093 \\ -1.2045 & 0.3221 & -1.3773 & 0.3683 \\ -0.3818 & -0.3093 & 0.3339 & 0.2705 \\ 1.3773 & -0.3683 & -1.2045 & 0.3221 \end{pmatrix}, \tag{5.1}$$

which gives the values

$$B_{235} = 0.193 \text{ T}, \tag{5.2}$$

$$L_{235} = 349.3 \text{ mm}. \tag{5.3}$$

```
import numpy as np

#Proton properties in SI units
m = 1.6726219*10**(-27);
q = 1.6021766208*10**(-19);
E = 75*10**3*q;
c = 2.99797458*10**8;
gamma = E/(m*c**2)+1;
betagamma = sqrt(gamma**2 - 1);
Er = m*c**2 #rest energy

#Solenoid constant
const_s = q/(2*m*c*betagamma);

#File reading function
def fieldMapToList(myfile):
f = open(myfile,'r')
traceWin = f.read().split('\n')

x = []
y = []
for pair in traceWin:
pair = pair.split(',')
x.append(float(pair[0].strip()))
y.append(float(pair[1].strip()))

return [x,y]
```

```
28
29 #Hard-edge model transfer matrix
30 def M_he(b,l):
31 k = b*const_s
32 s = sin(k*l)
33 c = cos(k*l)
34 if k != 0:
35 return Matrix([[c**2,s*c/k,s*c,s**2/k],
36 [-k*s*c,c**2,-k*s**2,s*c],
37 [-s*c,-s**2/k,c**2,s*c/k],
38 [k*s**2,-s*c,-k*s*c,c**2]])
39 else:
40 return Matrix([[1,0,0,0],
41 [0,1,0,0],
42 [0,0,1,0],
43 [0,0,0,1]])
```

Listing 5.6: Parameter settings and method definitions

```
1 #Read the field map
2 sol = fieldMapToList('Steerer/field_map_solenoid.txt')
3
4 #Redefine z to start at 0
5 length = sol[0][len(sol[0])-1]-sol[0][0]
6 sol[0] = [i-sol[0][0] for i in sol[0]]
7
8 #Fitting
9 p = numpy.polyfit(sol[0],sol[1],40)
10
11 #Calculating integral
12 q = numpy.polyint(p);
13
14 #Initiating matrix
15 M_sol = np.matrix([[1,0,0,0],[0,1,0,0],[0,0,1,0],[0,0,0,1]])
16
17 #Set segmentation parameters
18 N = 10000
19 dz = length/N
20 z = 0
21
22 #Calculate integral
23 for i in range(0,N):
24 I = numpy.abs(-numpy.polyval(q,z)+numpy.polyval(q,z+dz))
25 b = I/dz
26 M_sol = M_he(b,dz)*M_sol
27 z+=dz
28
29 print(M_sol)
30
31 #calculating new B and L
32 kl = np.arctan(np.float64(-M_sol[3,0]/M_sol[1,0]))
33 aux2 = np.sin(kl)**2
34 k = np.float64(M_sol[3,0])/aux2
35 B = k/const_s
36 L = kl/k
37
38 print([B,L])
```

Listing 5.7: Transfer matrix calculation via segmentation

Appendix III - IPAC conference abstract

Transverse dynamics and software integration of the ESS Low Energy Beam Transport

Sofia LOUISY, Natalia MILAS

Abstract: The first part of the ESS linac, which comprises the Ion Source and the Low Energy Beam Transport (LEBT) section, will be installed and commissioned already in early 2018. The LEBT is used to focus and correct the proton beam trajectory and clean the head and tail of the proton pulse from the flat top before entering the RFQ. Full beam characterization is planned during the ion source and LEBT commissioning at the RFQ entrance interface. It is thus important to have an application at the control room able to display quantities measured by the diagnostic devices and also to quickly run a simulation including not only centre of mass dynamics but also envelope. This paper presents the efforts in modelling the LEBT elements, as accurately as possible, and implementing the dynamics calculation and integration with diagnostics tools. The final result is a Java FX GUI based on the OpenXAL library.